



Power Electronic Systems  
Laboratory

© 2012 IEEE

Proceedings of the 38th Annual Conference of the IEEE Industrial Electronics Society (IECON 2012), Montreal, Canada,  
October 25-28, 2012

## Optimal Design of EMI Filters for Single-Phase Boost PFC Circuits

J. Mühlethaler,  
H. Uemura,  
J. W. Kolar

This material is published in order to provide access to research results of the Power Electronic Systems Laboratory / D-ITET / ETH Zurich. Internal or personal use of this material is permitted. However, permission to reprint/republish this material for advertising or promotional purposes or for creating new collective works for resale or redistribution must be obtained from the copyright holder. By choosing to view this document, you agree to all provisions of the copyright laws protecting it.



Eidgenössische Technische Hochschule Zürich  
Swiss Federal Institute of Technology Zurich

# Optimal Design of EMI Filters for Single-Phase Boost PFC Circuits

Jonas Mühlethaler, Hirofumi Uemura, and Johann W. Kolar  
 Power Electronic Systems Laboratory, ETH Zurich  
 Email: muehlethaler@lem.ee.ethz.ch

**Abstract**—Mains-connected boost power factor correction (PFC) circuits are employed in order to meet EMI standards. The EMI filter together with the boost inductor has to attenuate the high frequency (HF) voltage component to the mains side of the converter. In this paper, it is shown on the example of a single-phase PFC rectifier with nominal power  $P_N = 1.5$  kW, mains frequency  $f_{\text{mains}} = 50$  Hz, DC voltage  $V_{\text{DC}} = 400$  V, and mains voltage  $v_{\text{mains}} = 230$  V how the switching frequency and the relative ripple of the boost inductor current affect the filter and boost inductor volume and losses. With it, the optimum switching frequency and ratio of the ripple and fundamental current amplitude with respect to volume and losses is found.

## I. INTRODUCTION

Power electronic systems that are connected to the grid have to fulfill EMI standards concerning the level of DM EMI noise in the grid-side current, as e.g. Class A and Class B limits from CISPR [1], [2]. In order to meet such regulations, mains-connected boost power factor correction (PFC) circuits are employed. Together with an EMI input filter, they assure an approximate sinusoidal current waveform with power factors close to unity. A typical topology of a single-phase boost PFC rectifier is shown in Fig. 1(a). This topology has been discussed extensively in literature [3]–[6]. Such systems are designed for high efficiency and high power density; however, the increase of the power density often affects the efficiency, i.e. a trade-off between these two quality indices exists [7]. Depending on the application, the objectives efficiency and power density are weighted differently.

DM EMI noise is measured with a Line Impedance Stabilization Network (LISN) [2] which is connected between the grid and the power electronic system. An EMI Test Receiver is connected to the output of the LISN. The output of EMI Test Receiver is compared to the limits defined by the standards. Quasi-peak (QP) limits of the CISPR 11 standard are shown in Fig. 2.

In case of the single-phase PFC rectifier shown in Fig. 1(a), the EMI filter together with the boost inductor has to attenuate the high frequency (HF) component of the voltage  $v_{AB}$  to the mains side of the converter in order to meet the EMI standards. In Fig. 1(b) the structure of the applied filter is detailed. Since the filter may change the dynamics of the converter and may even increase the current ripple at the filter resonant frequency,  $L_d/R_{d1}$  and  $C_d/R_{d2}$  damping branches have been added. In [8] it is described how to optimally choose the damping branch components. Basically, there is a trade-off between the size of damping capacitor/inductor and the damping achieved. For this work,  $C_d = C_{\text{DM1}}$  and  $L_d = L_{\text{DM1}}$  have been selected as it showed to be a good compromise between additional

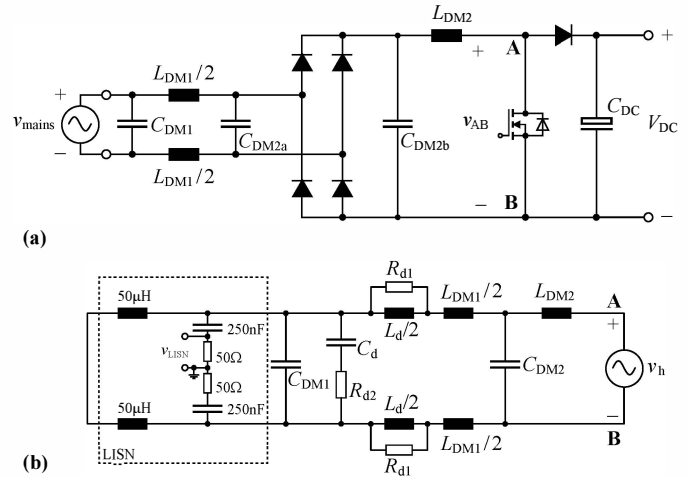


Fig. 1. (a) Single-phase PFC with boost inductor and input DM EMI filter. (b) Harmonics equivalent circuit, including LISN.

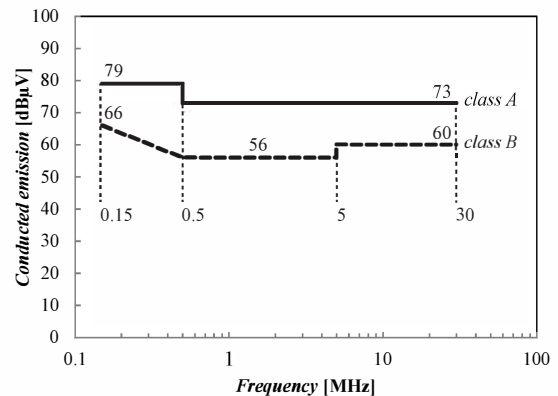


Fig. 2. Quasi-peak limits for conducted emissions at the mains parts of Class A equipments according to CISPR Publications 11.

volume needed and a reasonable damping achieved. The output voltage of the LISN  $v_{\text{LISN}}$  has to be within limits to meet EMI standards. For it, the transfer function  $v_{\text{LISN}}/v_{\text{AB}}$  has to attenuate the harmonics sufficiently.

In case of a large boost inductance  $L_{\text{DM2}}$ , a comparable small EMI filter ( $L_{\text{DM1}}$ ,  $C_{\text{DM1}}$ , and  $C_{\text{DM2}}$ ) is sufficient to meet the EMI standards. In return, when the boost inductance is selected small, and, accordingly, a high ripple current is accepted, the EMI filter must be designed larger. For a given frequency, an optimal ratio between ripple and fundamental

current exists at which the volume of the filter and boost inductor are minimized. It can be concluded similarly that, for each ripple ratio, an optimal frequency exists at which the volume is minimal. The ripple ratio is defined as the ratio of maximum (peak-to-peak) ripple current and (peak-to-peak) fundamental current  $k_i = \Delta I_{HF,max} / \Delta I_{LF}$ . The trade-off between boost inductor and filter volume, i.e. that there is an optimal  $f_P/k_i$ -combination, has been discussed in [9] already. In this paper, it is shown on the example of a single-phase PFC rectifier with nominal power  $P_N = 1.5$  kW, mains frequency  $f_{mains} = 50$  Hz, DC voltage  $V_{DC} = 400$  V, and mains voltage  $v_{mains} = 230$  V how the switching frequency and the ripple ratio affect the filter volume and losses. A focus is put on a simplified EMI modeling approach that considerably simplifies the analysis. Since the boost inductor also accounts for the attenuation of the high frequency (HF) component of the voltage  $v_{AB}$  to the mains side of the converter, it is, in the following discussion, considered to be part of the DM EMI filter.

First, in Section II a simplified DM EMI modeling is introduced which allows determining the required attenuation. Later, in Section III it is discussed how the inductors  $L_{DM1}$  and  $L_{DM2}$  are designed. In Section IV the single-phase PFC rectifier is explained in more details and results to the optimal designs are given.

## II. SIMPLIFIED EMI MODELING

A simplified EMI noise estimation is presented in [10], [11]. This simplified EMI modeling is based on the assumption that the total HF *rms* voltage at the LISN is an adequate measure for the estimation of the QP detection output voltage of the EMI Test Receiver.

The idea of the approach is illustrated in Fig. 3. All HF harmonic components of the voltage  $v_{AB}$  (cf. Fig. 1) are combined to a single harmonic component  $V_{h,rms}$  at the switching frequency  $f_P$ , i.e. the energy related to HF harmonics of  $v_{AB}$  of the switching frequency (including sidebands) and multiple of the switching frequency is considered to occur only at the switching frequency. This is an approximation, however, as in [10] shown, the error that results from this simplification is small. In the examples shown in [10], the error was always less than 6.7 dB. The major advantage of this simplification is that the calculation of this single harmonic component  $V_{h,rms}$  is very simple and can be conducted directly in the time domain, as will be shown later. Furthermore, since the total HF *rms* voltage at the LISN is an adequate measure for the estimation of the QP detection output voltage of the EMI Test Receiver, a model of the EMI Test Receiver is not needed.

The Class A and Class B limits from CISPR start at 150 kHz. Hence, if  $f_P < 150$  kHz,  $f_D = m \cdot f_P$  is the first frequency at which a harmonic component has to fulfill the standard.  $f_D$  is called the design frequency and  $m$  the rank of the first harmonic after 150 kHz. If  $f_P > 150$  kHz, it is  $f_D = f_P$ , accordingly. The estimated noise peak value at the design frequency  $f_D$  is  $m$  times smaller than  $V_{h,rms}$  for the case of rectangular voltage waveforms. The difference between the estimated value and the value of the EMI standards at frequency  $f_D$  defines the required attenuation of the filter.

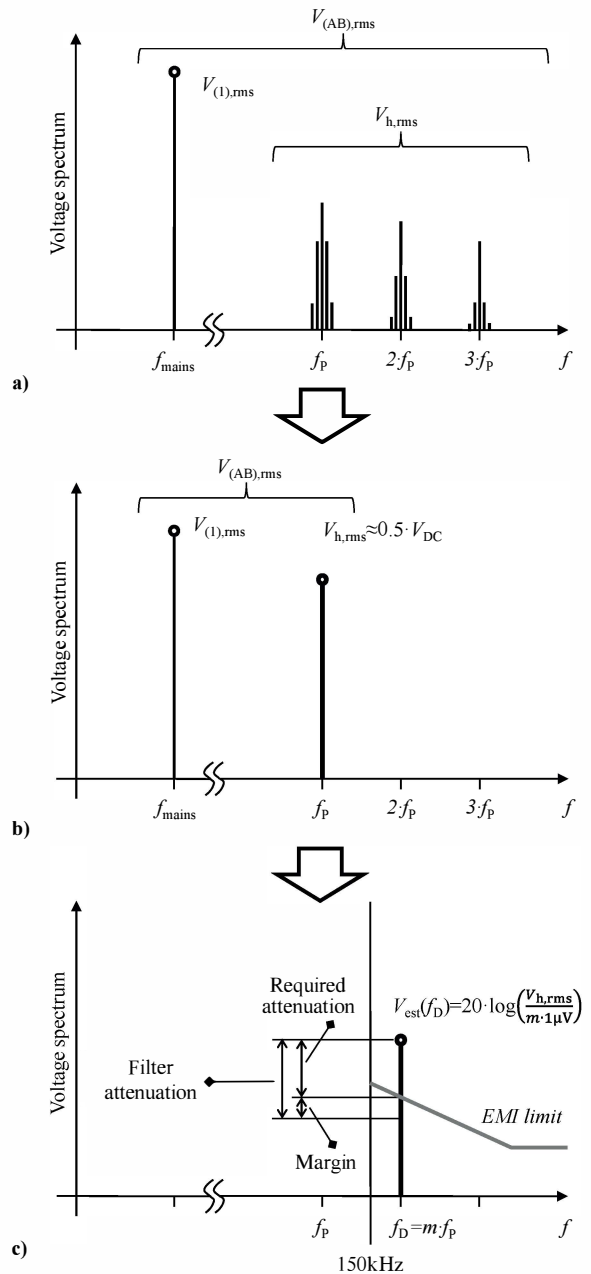


Fig. 3. Main idea of harmonic voltage estimation and filtering requirements.

The estimation of the required attenuation is separated into four steps which are explained below. All steps are illustrated in Fig. 3.

### 1) Determination of the DM EMI noise at switching frequency $f_s$

The filter's "input" voltage  $V_{AB,rms}$  consists of the fundamental voltage  $V_{(1),rms}$  and the DM EMI noise  $V_{h,rms}$ . Consequently, the *rms* value of the DM EMI noise can be calculated as

$$V_{h,rms} = \sqrt{V_{(AB),rms}^2 - V_{(1),rms}^2} \quad (1)$$

A worst case approximation of the DM EMI noise  $V_{h,rms}$  for the particular single-phase converter can be found in

[12] as

$$V_{h,rms} \approx 0.5 \cdot V_{DC}. \quad (2)$$

This rough approximation is valid since even a deviance by a factor of 2 would only mean a higher attenuation requirement of the EMI filter by 6 dB. For typical attenuation values in the range of 80...90 dB this is tolerable.

2) **Determination of the design frequency  $f_D$  and the rank  $m$**

The design frequency  $f_D$  of the first harmonic after 150 kHz is given by

$$f_D = m \cdot f_P \quad (3)$$

with the rank  $m$

$$m = \text{ceil}(150 \text{ kHz} / f_P), \quad (4)$$

where the function  $\text{ceil}$  represents the round-up operation.

3) **Estimation of the DM EMI noise at the design frequency  $f_D$**

The estimated noise peak value at the design frequency  $f_D$  is  $m$  times smaller than  $V_{h,rms}$  for the case of a rectangular voltage waveform. Hence, if no filter is considered, the voltage peak at the design frequency  $f_D$  in  $\text{dB}\mu\text{V}$  at the EMI Receiver can be estimated as

$$V_{\text{est}}(f_D)[\text{dB}\mu\text{V}] = 20 \cdot \log\left(\frac{V_{h,rms}}{m} \cdot \frac{1}{10^{-6} \text{ V}}\right). \quad (5)$$

4) **Calculation of the required attenuation  $Att_{\text{req}}$ :**

The required attenuation  $Att_{\text{req}}$  provided by the input filter (including boost inductor) in order to fulfill EMI standards is given by

$$\begin{aligned} Att_{\text{req}}(f_D)[\text{dB}] = & V_{\text{est}}(f_D)[\text{dB}\mu\text{V}] \\ & - Limit(f_D)[\text{dB}\mu\text{V}] \\ & + Margin[\text{dB}], \end{aligned} \quad (6)$$

where a  $Margin$  is added to be on the safe side. In the case at hand,  $Margin = 10 \text{ dB}$  has been chosen.

### III. DIMENSIONING OF INDUCTORS

The design of the inductors is important in order to find an optimal EMI filter design resulting in maximum filter efficiency or minimum filter volume. The design procedures of this section will be used in Section IV in order to analyze how the switching frequency and the ripple ratio affect the filter and boost inductor volume and losses. As mentioned before, the ripple ratio is defined as the ratio of maximum ripple current and fundamental current  $k_i = \Delta I_{\text{HF,max}} / \Delta I_{\text{LF}}$ . The boost inductor will be designed for an operation in continuous conduction mode (CCM), since, as will be shown later in Section IV, this is the optimal operating mode.

All inductors of this work are toroids with geometry illustrated in Fig. 4(a). The cores are made of iron powder from Micrometals. The material mix no. -18 has been selected for the optimization procedure. This material mix was selected because of its frequency characteristics; the permeability remains constant up to approximately 10 MHz. Litz wires of

copper are taken for the conductors of the boost inductor to reduce HF losses. For the filter inductors, since the HF current is reduced there, solid wires are taken. The modeling procedure is illustrated in Fig. 4(b). An optimization algorithm determines the optimal geometry parameter  $r_1$ ,  $r_2$ ,  $t$ ,  $d_a$ , and  $N$ . An inductor is optimal when the cost function

$$F = k_{\text{Loss}} \cdot q_{\text{Loss}} \cdot P + k_{\text{Volume}} \cdot q_{\text{Volume}} \cdot V \quad (7)$$

is minimized.  $k_{\text{Loss}}$ ,  $k_{\text{Volume}}$  are weighting factors,  $q_{\text{Loss}}$ ,  $q_{\text{Volume}}$  are proportionality factors, and  $P$ ,  $V$  are the filter losses and filter volume, respectively. The proportionality factors are chosen such that, for a "comparable performance",  $q_{\text{Loss}} \cdot P$  and  $q_{\text{Volume}} \cdot V$  are in the same range. The optimization algorithm has constraints as well as operating conditions that have to be met. The induction  $B_L$ , the inductor temperature  $T_L$ , and the inductor volume  $V_L$  are limited to  $B_{\text{max}}$ ,  $T_{\text{max}}$ , and  $V_{\text{max}}$ , respectively. The current in  $L$  has a fundamental (sinusoidal) component, with an amplitude  $I_{\text{LF,p}}$  and frequency of  $f_{\text{LF}}$ , and a superimposed ripple current. The ripple current is, for the purpose of simplification, for the optimization considered to be sinusoidal with constant amplitude  $I_{\text{HF,p}}$  and frequency  $f_{\text{HF}}$  over the mains period. The losses for the fundamental and the high-frequency ripple are calculated independently, and then summed.

The loss modeling is based on the framework introduced in [13]. The modeling steps (1) to (4) illustrated in Fig. 4(b) are discussed in the following.

#### A. Calculation of the Inductance

The inductance of a toroid is calculated as

$$L = N^2 \mu_r \mu_0 \frac{A_e}{l_e}, \quad (8)$$

where  $N$  is the number of winding turns,  $\mu_r$  the relative permeability,  $\mu_0$  the magnetic field constant,  $A_e$  the effective cross-sectional area, and  $l_e$  the effective magnetic length. The effective dimensions of a toroid can be calculated as e.g. given in [13], [14]. The relative permeability  $\mu_r$  is defined by the (nonlinear)  $BH$ -relation of the core material, i.e. it has to be extracted from the material data sheet in order to calculate the inductance as a function of the current.

For CCM, the required boost inductance value for a particular ripple current is given as [4]

$$L_{\text{CCM}} = \frac{V_{\text{DC}}}{4f_P \Delta I_{\text{HF,max}}}, \quad (9)$$

with the maximum current ripple  $\Delta I_{\text{HF,max}}$ . In CCM, the maximum current ripple occurs at half the fundamental peak current, i.e. the nominal boost inductance value  $L_N = L_{\text{CCM}}$  has to be met at half the current  $\hat{I}_{\text{LF}}/2$  accordingly. It is guaranteed that the boost inductance at the peak current never drops below 60% of the nominal inductance  $L_N$ . The filter inductance, however, has to meet the nominal inductance value (which is determined differently) up to  $\hat{I}_{\text{LF}}$ , since it has to provide the required damping over the full current range.

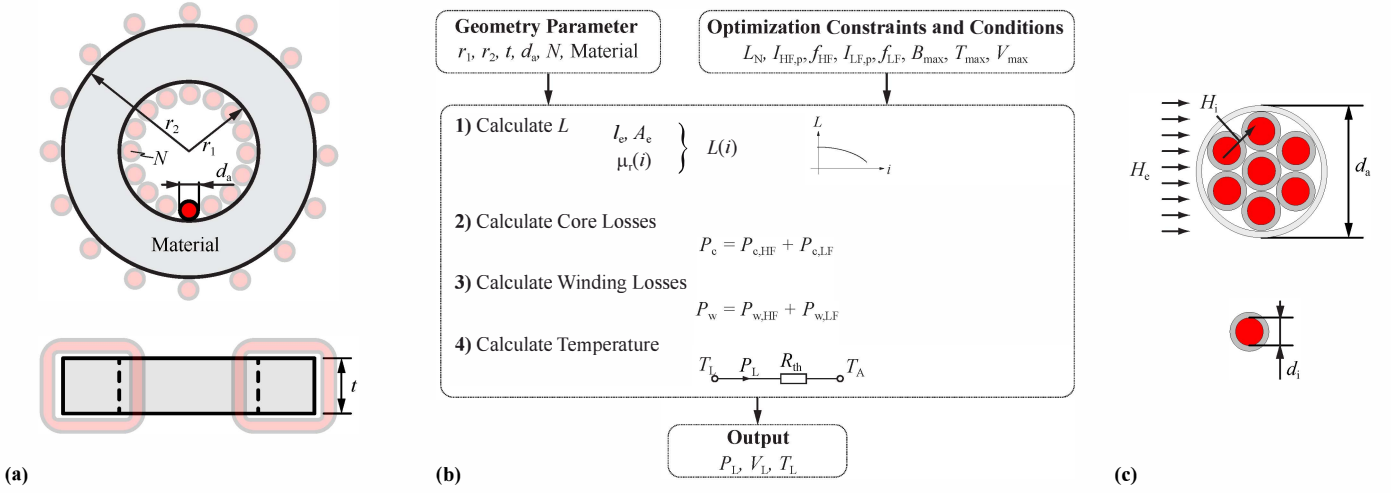


Fig. 4. (a) Geometry of inductors employed in the input filter. (b) Modeling Procedure. (c) Cross-sectional area of litz-wire winding.

### B. Core Losses

The core losses are calculated for the low-frequency fundamental and for the high-frequency ripple independently and then summed. The calculation has been made with the core loss curve-fit formula provided by Micrometals<sup>1</sup>.

### C. Winding Losses

The second source of losses in inductive components are the ohmic losses in the windings. The skin-effect losses, including DC losses, of a litz-wire winding that consists of  $n$  strands, each with strand diameter  $d_i$  (cf. Fig. 4(c)) are calculated as [15], [16]

$$P_{S,L} = n \cdot R_{\text{DC}} \cdot F_R(f) \cdot \left( \frac{\hat{I}}{n} \right)^2, \quad (10)$$

where  $R_{\text{DC}} = 4/(\sigma \pi d_i^2)$ .  $F_R(f)$  is calculated with the strand diameter  $d = d_i$ . The equation for  $F_R(f)$  can be found e.g. in [13], [15], [16]. The strand diameter has been selected to be the same as the skin depth, i.e.  $d_i = 1/\sqrt{\pi \mu_0 \sigma f}$ , where  $\mu_0$  is the magnetic field constant and  $\sigma$  electric conductivity of copper. In (10) litz-wire bundle-level effects (e.g. discussed in [17], [18]) are neglected.

The magnetic field that leads to proximity-effect losses is the sum of the external magnetic field  $H_e$  and the internal magnetic field  $H_i$  (cf. Fig. 4(c)). The proximity-effect losses in litz-wire windings can then be calculated as [13], [15], [16]

$$P_{P,L} = n \cdot R_{\text{DC}} \cdot G_R(f) \left( H_e^2 + \frac{\hat{I}^2}{2\pi^2 d_a^2} \right) \quad (11)$$

where  $G_R(f)$  is calculated with the strand diameter  $d = d_i$ . The equation for  $G_R(f)$  can be found e.g. in [13], [15], [16].  $d_a$  is the litz-wire diameter as illustrated in Fig. 4(c).

For the calculation of the external field  $H_e$  of the boost inductor, the winding window is assumed to be filled with conductors and each conductor is assumed to be penetrated by the average external magnetic field. This assumption is similar

to the one made to calculate the internal magnetic field  $H_i$  of litz wires [15], [16]. The square of the external field  $H_e$  for (11) is then

$$H_e^2 = \frac{(N\hat{I})^2}{2\pi^2(2r_1)^2}. \quad (12)$$

In order to improve the frequency characteristic of the filter inductors, their winding is wound on a single layer. This simplifies the calculation of the external field; it can be calculated directly with Ampere's Law. The filter inductors are, furthermore, made of solid wire. Accordingly, in (10) and (11)  $n = 1$  has to be selected and in (11) the second summand in the brackets is ignored.

### D. Thermal Modeling

A thermal model is important when minimizing the filter volume, as the maximum temperature allowed is the limiting factor when reducing volume. The model used in this work consists of only one thermal resistance  $R_{\text{th}}$  and is illustrated in Fig. 4(b). The inductor temperature  $T_L$  is assumed to be homogenous; it can be calculated as

$$T_L = T_A + P_L R_{\text{th}}, \quad (13)$$

where  $P_L$  are the total losses occurring in the inductor, consisting of core and winding losses, and  $T_A$  is the ambient temperature. The ambient temperature  $T_A$  is assumed to be constant at 25 °C. The heat transfer is mainly due to convection. Radiation as a heat transfer mechanism has been neglected. Details about thermal modeling are not given here; the interested reader is referred to [19], from where the formulas used in this work have been taken.

### E. Result

The optimization procedure leads to different inductor designs depending on the chosen weighting factors  $k_{\text{Loss}}$  and  $k_{\text{Volume}}$  in (7), i.e. depending whether the aim of the optimization is more on reducing the volume  $V$  or more on reducing the losses  $P$ . Limiting factors are the maximum temperature  $T_{\text{max}}$  (limits the volume from being too low) and a

<sup>1</sup>www.micrometals.com, 23.2.2012

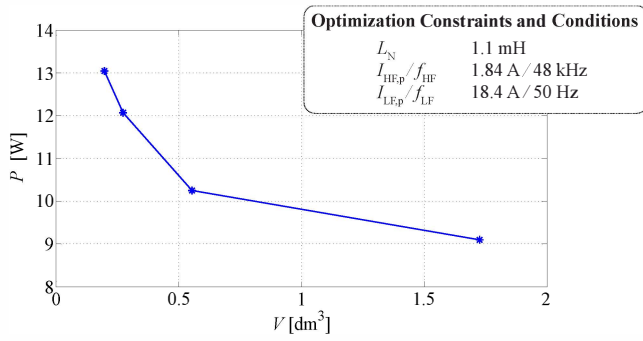


Fig. 5. Filter volumes  $V$  and filter losses  $P$  of different optimal boost inductor designs.

maximum volume  $V_{\max}$  (limits the efficiency from being too high). Different boost inductor designs to one optimization task are shown by a  $P$ - $V$ -plot, i.e. a  $P$ - $V$ -Pareto front in Fig. 5; the trade-off between losses and volume can be clearly identified.

#### IV. OPTIMAL DESIGN OF THE EMI FILTER

The single-phase PFC rectifier investigated in this work is shown in Fig. 1. As mentioned before, since the boost inductor also accounts for the attenuation of the HF component of the voltage  $v_{AB}$  to the mains side of the converter, it is, in the following discussion, considered to be part of the DM EMI filter. The goal is to optimally select and design the DM filter components. As discussed in the introduction, there presumably exists an optimal frequency and an optimal ripple ratio for a given operating point. The most common operating modes for boost power factor correction are the continuous conduction mode (CCM) and the discontinuous condition mode (DCM); the modes are illustrated in Fig. 6(a) and (b). For the sake of brevity, they are not explained in detail in this paper and the reader is referred to [20] for more information. The boundary between CCM and DCM conduction mode can be determined as [6]

$$f_P \cdot L_{DM2} = \frac{(\sqrt{2}v_{\text{mains}})^2}{4P} \cdot \left(1 - \frac{v_i}{V_{DC}}\right), \quad (14)$$

with the boost inductance  $L_{DM2}$ , the switching frequency  $f_P$ , the output voltage  $V_{DC}$ , the output power  $P$ , and the input voltage  $v_i = \sqrt{2}v_{\text{mains}} \cdot \sin \omega t$ . The right side of (14) is plotted in Fig. 6(c) for  $V_{DC} = 400$  V and  $P = 1500$  W. In case the product  $f_P \cdot L_{DM2}$  is always (i.e. for a full mains period) above the curve in Fig. 6(c), CCM is guaranteed; as soon the product goes below the curve at some instant, the rectifier operates (partly) in DCM mode. In DCM the boost inductor can be selected smaller, however, in return, the filter must be designed larger. It has to be analyzed what mode is favorable for a particular operating point.

As mentioned before, for CCM, the required inductor value for a particular ripple current is given as [4]

$$L_{CCM} = \frac{V_{DC}}{4f_P \Delta I_{HF, \max}}, \quad (15)$$

with the maximum current ripple  $\Delta I_{HF, \max}$ . (which occurs at  $\pi/4$  of the mains period).

In the following, on the example of the single-phase PFC rectifier illustrated in Fig. 1(a) (nominal power  $P_N = 1.5$  kW, mains frequency  $f_{\text{mains}} = 50$  Hz, DC voltage  $V_{DC} = 400$  V, and mains voltage  $v_{\text{mains}} = 230$  V), it is shown how the switching frequency  $f_P$  and the ripple ratio  $k_i$  affect the filter volume and losses. EMI filters are designed for different combinations of switching frequencies and ripple ratios  $f_P/k_i$ . Each filter design is performed to aim for low volume or low losses, while guaranteeing the attenuation to meet the CISPR 11 class B standard. The capacitance density to calculate the capacitors volume are approximated with  $0.05 \mu\text{F}/\text{cm}^3$  (based on the WIMA MKP-X2 film capacitor series). The inductors are designed as toroids of iron powder from Micrometals as introduced in Section III.

With (15) the boost inductance value can be calculated for a given  $f_P/k_i$ -combination. The boost inductor is then optimally designed as discussed in Section III. Furthermore, the attenuation that is required from the part of the filter consisting of  $L_{DM1}$ ,  $C_{DM1} = C_{DM1a} + C_{DM1b}$ , and  $C_{DM2}$  can be calculated. An optimization algorithm determines the optimal capacitance values  $C_{DM1}/C_{DM2}$  as well as the optimal geometry parameter  $r_1$ ,  $r_2$ ,  $t$ ,  $d_a$ , and  $N$  of  $L_{DM1}$ . In so doing, the CLC filter is optimally designed such that the filter achieves the required attenuation, while low losses or minimum volume is guaranteed. This is repeated for different  $f_P/k_i$ -combinations in order to find the optimum combination.

The results for volumetric optimized designs are given in Fig. 7. When the frequency  $f_P$  is kept constant, and the ripple ratio  $k_i$  is varied, the filter volume share between the boost inductor  $L_{DM2}$  and the rest of the filter, i.e. the filter part consisting of  $L_{DM1}$ ,  $C_{DM1} = C_{DM1a} + C_{DM1b}$ , and  $C_{DM2}$ , changes. This is illustrated in Fig. 8(a). As can be seen, an increase of  $k_i$  at low values of  $k_i$  reduces the volume of the boost inductor; however, then a further increase of  $k_i$  leads to larger boost inductors. The reason for this increase are, presumably, the large HF losses that have to be dissipated and, accordingly, a higher inductor surface is required. There is, for each frequency, an optimal  $k_i$  at which the filter volume is reduced.

A similar conclusion can be made when  $k_i$  is kept constant and the frequency  $f_P$  is varied. This is illustrated in Fig. 8(b). The lower the switching frequency  $f_P$ , the larger the boost inductor  $L_{DM2}$ ; and, the lower the switching frequency  $f_P$  the smaller the  $C_{DM2}/L_{DM1}/C_{DM1}$ -part of the filter. There is, for each  $k_i$ , an optimal frequency  $f_P$ . The size of the  $C_{DM2}/L_{DM1}/C_{DM1}$ -part of the filter is not a continuous function of the frequency. As can be seen in Fig. 8(b), the filter size steps always when the rank  $m$  changes<sup>2</sup>. As long the rank remains constant, an increase of the switching frequency leads to (slightly) lower  $CLC$ -volumes. For instance, the  $CLC$ -volume drops between 75 kHz and 150 kHz. Consequently, the optimum switching frequency is always just below a frequency at which the rank  $m$  changes. In the example at hand, this is at 144 kHz (the evaluated frequency that is closest below 150 kHz).

In Fig. 7(b) the losses to the designs are given. It can be seen that more voluminous designs have higher losses. This is

<sup>2</sup> $m$  is the rank of the first harmonic after 150 kHz (cf. Section II).

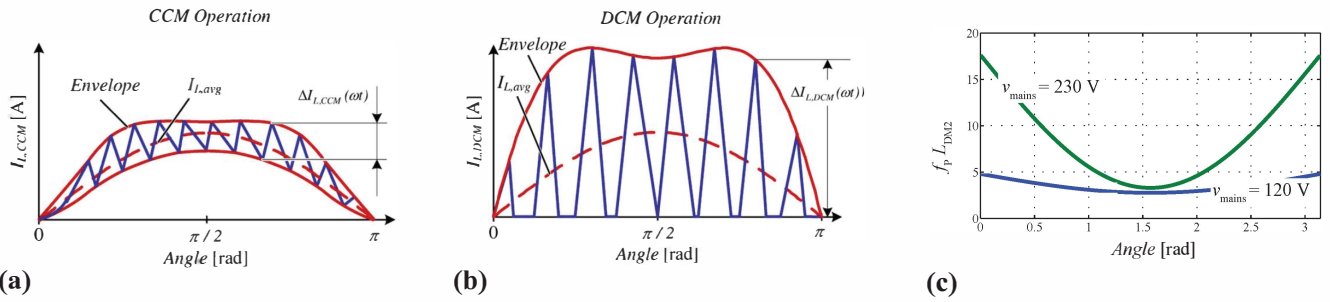


Fig. 6. (a) Current waveform in CCM (Figure from [4]); (b) Current waveform in DCM (Figure from [4]); (c) CCM-borderline of  $f_p \cdot L_{DM2}$  within a mains half wave [6].

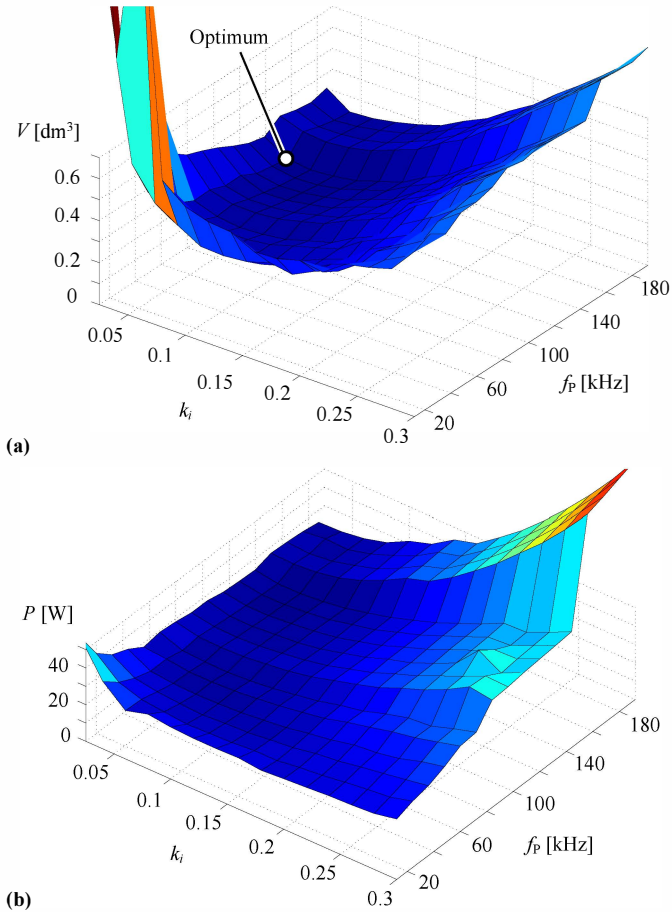


Fig. 7. (a) Impact of switching frequency and ripple ratio  $k_i$  on filter volume (results to volumetric-optimized designs). (b) Power losses to the designs of (a). The resolutions in  $f$  and  $k_i$  are  $\Delta k = 0.02$  and  $\Delta f_P = 12$  kHz.

obvious, since all designs are at the thermal limit, higher losses are tolerable with a higher volume, as the surface for the heat dissipation increases with increasing volume. The converter operates in CCM in all  $f_p/k_i$ -combinations investigated in Fig. 7; hence, CCM is the favorable mode in the case at hand.

An overall optimal  $f_p/k_i$  combination can be found; in Fig. 9(a) this operating point is detailed. A simulation model<sup>3</sup>

<sup>3</sup>Simulation Software: GeckoCIRCUITS - v1.54 (www.gecko-research.com)

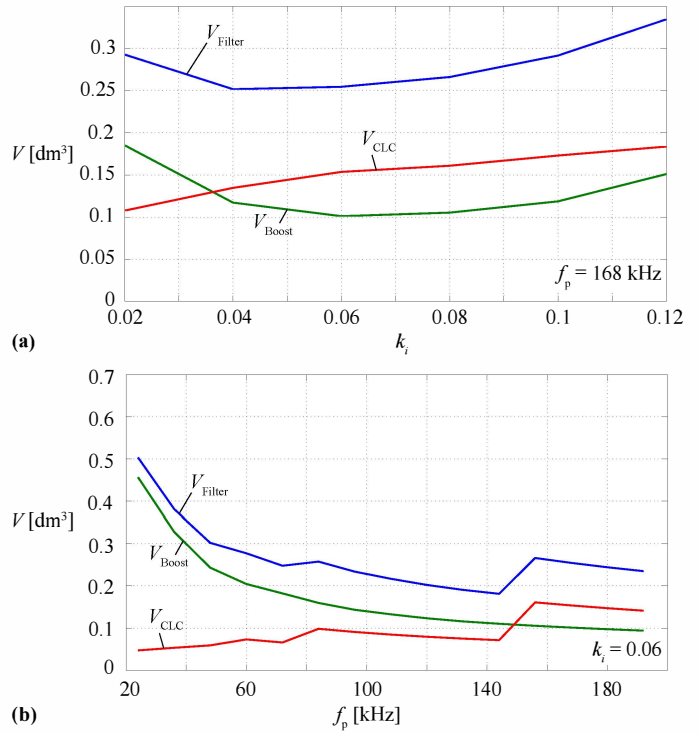


Fig. 8. (a) The filter volume share as a function of the ripple ratio  $k_i$  when the frequency  $f_p = 168$  kHz is kept constant. (b) The filter volume share as a function of the frequency  $f_p$  when the ripple ratio  $k_i = 0.06$  is kept constant.

of the investigated PFC rectifier has been set up. Simulated conducted emission results are given in Fig. 9(b). As can be seen, the conducted emissions are always within the tolerable limits. The reached margin of approximately 8.2 dB $\mu$ V is very close to the margin added in (6), i.e. the simplified calculation was very accurate.

In the example of Fig. 7, the filter volume was minimized under thermal constraints. However, the increase of the power density (i.e. reduction of volume) affects the efficiency. As mentioned in the introduction, a trade-off between these two quality indices exists. Depending on the application, the objectives efficiency and power density are weighted differently. An objective could be to select the filter components such that, for a given filter volume  $V_{max}$ , the losses in the filter are minimized. In Fig. 10 results of loss-optimized designs

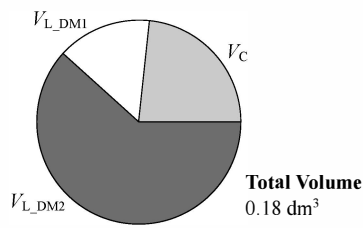
### Operating Point

$f_P$  144 kHz  
 $k_i$  0.06  
 Attenuation 109 dB

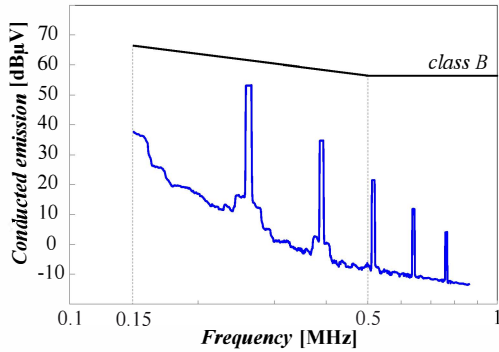
### Filter Values

$L_{DM1} = 42 \mu\text{H}$   
 $L_{DM2} = 0.63 \text{ mH}$   
 $C_{DM1} = C_{DM2} = 0.70 \mu\text{F}$

### Volume Partitioning



(a)



(b)

Fig. 9. (a) Details to overall optimal design. (b) EMI simulation results.

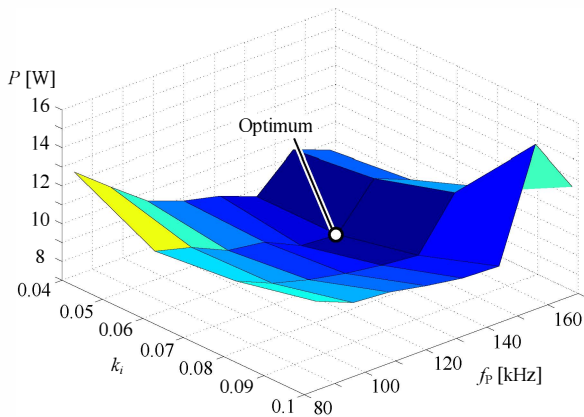


Fig. 10. Results to the loss-optimized / volumetric-limited optimization ( $V_{\max} = 0.4 \text{ dm}^3$ ). Optimum at  $k_i = 0.06$  and  $f_P = 144 \text{ kHz}$ . The resolutions in  $f$  and  $k_i$  are  $\Delta k = 0.02$  and  $\Delta f_P = 12 \text{ kHz}$ .

are given. The volume was limited to  $0.4 \text{ dm}^3$ . It can be seen that the optimal combination of  $f_P/k_i$  is the same as the one of the volumetric optimal design. An explanation of this behavior is that the volume difference between volumetric optimized designs and the limit  $V_{\max}$  is maximal for the point of volumetric optimal design; thus, the losses can be reduced most at this point.

## V. CONCLUSION AND FUTURE WORK

Mains-connected boost power factor correction (PFC) circuits are employed in order to meet EMI standards. In this paper, it was shown on the example of a single-phase PFC rectifier with nominal power  $P_N = 1.5 \text{ kW}$ , mains frequency  $f_{\text{mains}} = 50 \text{ Hz}$ ,  $V_{DC} = 400 \text{ V}$ , and  $v_{\text{mains}} = 230 \text{ V}$  how the

switching frequency and the ripple ratio affect the design of the EMI filter, including boost inductor. With it, the optimum switching frequency and ripple ratio with respect of volume and losses is found. A focus was put on a simplified EMI modeling approach that considerably simplifies the analysis.

As a future task, an overall system optimization including the power semiconductors and DC link capacitor in order to determine the overall optimum could be conducted.

## REFERENCES

- [1] M. L. Heldwein, *EMC Filtering of Three-Phase PWM Converters*. PhD thesis, ETH Zurich, 2008.
- [2] *Specification for Industrial, scientific and medical (ISM) radio-frequency equipment - Electromagnetic disturbance characteristic - Limits and methods of measurement - Publication 11*. IEC International Special Committee on Radio Interference - C.I.S.P.R. Std., 2004.
- [3] J. Zhang, J. Shao, P. Xu, F. C. Lee, and M. M. Jovanovic, "Evaluation of input current in the critical mode boost PFC converter for distributed power systems," in *Proc. of Applied Power Electronics Conf. and Exposition APEC*, vol. 1, pp. 130–136, 2001.
- [4] T. Nussbaumer, K. Raggl, and J. W. Kolar, "Design guidelines for interleaved single-phase boost PFC circuits," vol. 56, no. 7, pp. 2559–2573, 2009.
- [5] K. Raggl, T. Nussbaumer, G. Doerig, J. Biela, and J. W. Kolar, "Comprehensive design and optimization of a high-power-density single-phase boost PFC," vol. 56, no. 7, pp. 2574–2587, 2009.
- [6] M. Albach and D. Dambois, "Optimized operation mode for 3 kw off-line preconditioner circuits," in *Proc. of European Power Electronics Conf. (EPE), Florence, Italy*, pp. 134–139, 1991.
- [7] J. W. Kolar, J. Biela, S. Waffler, T. Friedli, and U. Badstuebner, "Performance trends and limitations of power electronic systems," in *Proc. of the 6th International Conference on Integrated Power Electronics Systems (CIPS)*, pp. 1–20, 2010.
- [8] R. W. Erickson and D. Maksimovic, *Fundamentals of Power Electronics*. Springer Science+Business Media, LLC, 2004.
- [9] J. Zientarski, R. Beltrame, D. Candido, M. da S. Martins, and H. Hey, "Design methodology for universal line input boost power factor correction magnetics," *IET Power Electronics*, vol. 4, pp. 715–724, July 2011.
- [10] K. Raggl, T. Nussbaumer, and J. W. Kolar, "Guideline for a simplified differential-mode EMI filter design," *IEEE Transactions on Industrial Electronics*, vol. 57, pp. 1031–1040, March 2010.
- [11] B. Cougo, T. Friedli, D. O. Boillat, and J. W. Kolar, "Comparative evaluation of individual and coupled inductor arrangements for input filters of PV inverter systems," in *Proceedings of the International Conference of Integrated Power Electronics Systems (CIPS 2012)*, March 2012.
- [12] J. W. Kolar, F. Krismer, Y. Lobsiger, J. Mühlethaler, T. Nussbaumer, and J. Miniböck, "Extreme efficiency power electronics," in *Proc. of the International Conference of Integrated Power Electronics Systems (CIPS), Nuremberg, Germany*, 2012.
- [13] J. Mühlethaler, J. W. Kolar, and A. Ecklebe, "Loss modeling of inductive components employed in power electronic systems," in *Proc. of the 8th International Conference on Power Electronics - ECCE Asia*, pp. 945–952, 2011.
- [14] E. C. Snelling, *Soft Ferrites, Properties and Applications*. 2<sup>nd</sup> edition, Butterworths, 1988.
- [15] J. Biela, *Optimierung des elektromagnetisch integrierten Serien-Parallel-Resonanzkonverters mit eingepprägtem Ausgangsstrom*. PhD thesis, ETH Zurich, 2005.
- [16] J. A. Ferreira, *Electromagnetic Modelling of Power Electronic Converters*. Kluwer Academic Publishers, 1989.
- [17] C. Sullivan, "Optimal choice for number of strands in a litz-wire transformer winding," *IEEE Transactions on Power Electronics*, vol. 14, pp. 283–291, Mar. 1999.
- [18] H. Rossmann, M. Doebroenti, M. Albach, and D. Exner, "Measurement and characterization of high frequency losses in nonideal litz wires," *IEEE Transactions on Power Electronics*, vol. 26, no. 11, pp. 3386–3394, 2011.
- [19] *VDI Heat Atlas*. Springer-Verlag Berlin Heidelberg, 2010.
- [20] L. Rossetto, G. Spiazzi, and P. Tenti, "Control techniques for power factor correction converters," in *Proc. of PEMC, Warsaw, Poland*, pp. 1310–1318, 1994.